Journal of Cluster Science (2019) 30:973–984
https://doi.org/10.1007/s10876-019-01557-0

ORIGINAL PAPER

# Incorporation of Keggin-Type Phosphomolybdic Acid, Ionic Liquid and Carbon Nanotube Leading to Formation of Multifunctional Ternary Composite Materials: Fabrication, Characterization and Electrochemical Reduction/Detection of Iodate, Borate and Nitrite

Ting Wang[1] · Qingcheng Zhou[1] · Xiaoyu Ren[1] · Yunshan Zhou[1] · Lijuan Zhang[1] · Farooq K. Shehzad[1] · Arshad Iqbal[1]

Received: 8 February 2019 / Published online: 16 April 2019


## Abstract

Single wall carbon nanotube substituted ionic liquids were synthesized successfully by esterification reaction of the carboxylated single wall carbon nanotubes (SWNTs) with hydroxyl ammonium ionic liquids (ILs) of the formula $CH_3N(CH_2CH_2OH)_2(C_nH_{2n+1})Br$ (n = 4, 8, 12), which subsequently reacted with molybdophosphoric acid ($PMo_{12}$) to form three new ternary composite materials (SWNTs-$ILC_n$-$PMo_{12}$) (n = 4, 8, 12). The composites modified glass carbon electrodes were used to study electrochemical properties systematically through cyclic voltammetry method. The results showed that electronic conductivity of SWNTs moiety and ionic conductivity of ILs moiety in the composite materials played important roles in the electrochemistry and electrocatalysis. The length of alkyl carbon chain of the ionic liquids in the composite materials was also found to influence the electrochemical properties. The experimental results also showed that all the composites modified electrode can catalytically reduce and detect $IO_3^-$, $BrO_3^-$ and $NO_2^-$ with very high efficiency (low detection limit, short response time and wide linear range).

**Keywords** Composite materials · Preparation · Electrochemical reactons · Sensor

## Introduction

Ionic liquids (ILs) are a class of low-melting salts that have good ionic conductivity and broad electrochemical window [1], non-volatile, recyclable, and are free of any molecular solvent [2]. These excellent physical properties make them a fascinating material with considerable interests in green chemistry. In addition, the functionalization of ionic liquids has become the focus of current attention [3–6]. Through the functional modification of the anionic/cationic ions constituting the ILs, they can also be used as a catalyst or a reaction reagent in addition to being used as a solvent [7]. Theoretically, both cationic and anionic moieties of ILs can be functionally modified. However, from the current research results, functional modifications of ILs are mostly concentrated in the cation part and are achieved by modifying atoms such as nitrogen [3] and phosphorus [4] or heterocyclic rings such as imidazole [5] and pyridine [6], but the functional modifications of anion are less studied [8].

On the other hand, polyoxometalates (POMs) are a class of multinuclear complexes that have attracted wide attention due to their diversity of sizes, compositions and functions [9]. They are widely used in electrocatalysis [10, 11], electrochemical sensors [12, 13] and others owing to their stable redox states, and they can undergo reversible, multi-steps, multi-electrons transfer reactions. The

**Electronic supplementary material** The online version of this article (https://doi.org/10.1007/s10876-019-01557-0) contains supplementary material, which is available to authorized users.

✉ Yunshan Zhou
zhouys@mail.buct.edu.cn

✉ Lijuan Zhang
ljzhang@mail.buct.edu.cn

[1] State Key Laboratory of Chemical Resource Engineering, Institute of Science, Beijing University of Chemical Technology, Mailbox 99, 15 Beisanhuan East Road, Beijing 100029, People's Republic of China

use of polyoxometalate to modify IL is expected to enable the development of novel functional ionic liquids in the field of electrocatalysis and electrochemical sensors. In recent years, there have been a few reports on the synthesis of novel ionic liquid-polyoxometalate (IL-POM) composites. Kim et al. [14] developed a hybrid electrolyte which was synthesized by phosphotungstic acid ($PW_{12}$) and ionic liquids ([BMIM][TFSI]), and its conductivity is higher than the original components. Wu et al. [15] presented two thermoresponsive POM/IL supramolecular gel electrolytes for supercapacitors, which are $[TBTP]_5PW_{10}V_2O_{40}$ and $[TBTP]_8P_2W_{16}V_2O_{62}$, and there is a significant improvement in the conductivity, thermal performance, and a lower phase inversion temperature.

In addition, IL can interact strongly with carbon nanotubes through "cation-π" forces [16], which can effectively inhibit the binding between the carbon nanotubes themselves. Due to the extremely low toxicity of the ionic liquid to the high conductivity of the carbon nanotubes, it is advantageous to demonstrate its excellent electrochemical properties. Recently, the combination of carbon nanotubes and ionic liquids and their applications have been studied in various ways. Sun et al. [17] developed a novel, simple, one-step coelectrodeposition method to deposit Ni and MWNTs in IL with a rapid response time and a low detection limit for non-enzymatic glucose sensing. Li et al. [18] presented a reliable method based on a MWNTs modified carbon ionic liquid electrode that has been successfully applied for determination of dopamine in the presence of ascorbic acid. Impressively, Niu et al. innovatively used the carboxyl groups of single-walled carbon nanotubes to react with amine groups of imidazole-type ionic liquids to form amide bonds, and then ionic liquids and polyoxometalates were ionically bonded to prepare composite SWNTs-IL-$PMo_{12}$, which achieve the modification of two parts of ions of ionic liquid. The resulting ternary complex has high stability, excellent wettability and fast electron transfer activity [19]. Behzad et al. also developed a robust and stable film GCE/MWCNTs/$[C_8Py][PF_6]$-$PMo_{12}$ by dip-coating in an acetonitrile solution containing $[C_8Py][PF_6]$ and $PMo_{12}$, which showed great electrocatalytic activity towards the reduction of $H_2O_2$ and iodate. The modified electrode showed the ability for iodate detection including low detection limit (0.02–2 mM), high sensitivity (14.81 μA $mM^{-1}$), short response time (< 2 s) and satisfactory linear concentration range [20]. Based on the above reports, it can be concluded that taking the advantage of the SWNTs, IL and POM components each has excellent characteristics, the resulting ternary composites may not only maintain the great performance of each components, but also may generate a synergistic effect due to the interaction. Thus, there is no doubt that much more effort is greatly required to develop such new ternary composites in both theoretical and practical view for development of new type of environment-friendly functional materials.

In this paper, two-component composites SWNT-$ILC_n$ (n = 4, 8, 12) were firstly prepared by the esterification reaction between the carboxyl groups of carboxylated single-walled carbon nanotubes (SWNTs) and the hydroxyl functional groups of the ethanolamine ILs of formula $CH_3N(CH_2CH_2OH)_2(C_nH_{2n+1})$ Br (n = 4, 8, 12), afterwards the $Br^-$ of the composites was exchanged with negatively charged polyoxometalate anions $PMo_{12}O_{40}^{3-}$ ($PMo_{12}$), leading to formation of three new ternary composites SWNTs-$ILC_n$-$PMo_{12}$ (n = 4, 8, 12), in which the anion and cation moieties of ethanolamine ionic liquids are all functionalized. Their electrochemical properties were systematically studied by cyclic voltammeter after spin-coating the composites on glassy carbon electrodes and the resulting electrodes SWNTs-$ILC_n$-$PMo_{12}$ (n = 12) showed the best sensor performances for reducing/detecting iodate, bromate and nitrite with low detection limit, short response time and wide linear range.

## Experimental

### Materials and Methods

Carboxylated single-walled carbon nanotubes (SWNTs) (Carboxylation rate: 2.73%) was purchased from Chengdu Organic Chemicals Co. Ltd, Chinese Academy of Sciences. All the starting materials were obtained from Aladdin and Macklin. They were analytical grade with high purity, and were employed with no further purification. $H_2SO_4/Na_2SO_4$ solution of different pH values were directly prepared from $H_2SO_4$ (0.5 mol/L) and NaOH (1 mol/L). $CH_3N(CH_2CH_2OH)_2C_{12}H_{25}Br$ ($ILC_{12}$) [21], $CH_3N(CH_2CH_2OH)_2C_8H_{25}Br$ ($ILC_8$) [22], $CH_3N(CH_2CH_2OH)_2C_4H_{25}Br$ ($ILC_4$) [22] were prepared according to the literature methods.

Fourier transform infrared (FT-IR) spectra were recorded on a Bruker Vector 22 infrared spectrometer with KBr pellets in the range of 400–4000 $cm^{-1}$. Elemental analyses for C, H, N were performed on a Perkin-Elmer 240C analytical instrument. Thermogravimetric analyses were performed on a TGA-50 instrument at a heating rate of 10 °C $min^{-1}$ under ambient conditions atmosphere. Electrochemical measurement was carried out on a CHI-660 electrochemical workstation at room temperature. All solutions were deaerated by bubbling highly pure argon prior to experiments and the electrochemical cells like reference electrode: Ag/AgCl (saturated KCl), work electrode: functional glassy carbon electrode (diameter 3 mm), and a platinum wire counter electrode were kept under

argon atmosphere throughout these experiments. The glassy carbon working electrodes were polished with alumina on polishing pads, rinsed with ethanol/$H_2O$ (1:1) solution, concentrated nitric acid/$H_2O$ (1:1) solution and distilled water. At last the electrodes were sonicated in $H_2O$ and used for the study of electrochemistry and electrochemical reduction/detection of iodate, borate and nitrite.

### Preparation of $(CH_3N(CH_2CH_2OH)_2C_nH_{2n+1})_3PMo_{12}O_{40}$ ($ILC_n$-$PMo_{12}$: n = 4, 8, 12)

*Preparation of $(CH_3N(CH_2CH_2OH)_2C_{12}H_{25})_3PMo_{12}O_{40}$ ($ILC_{12}$-$PMo_{12}$)* $ILC_{12}$ (1.8 mmol, 0.663 g) was dissolved in 10 mL of water and added drop-wise to a phosphomolybdic acid (0.6 mmol, 1.095 g) aqueous solution (10 mL) under stirring for 1 h, The resulting product obtained was washed with distilled water and dried in air. Elemental analysis calcd. (%): C, 22.78; N, 1.56; H, 4.24. Found (%) C, 22.12; N, 1.42; H, 4.11. Yield, 0.13 g.

*Preparation of $(CH_3N(CH_2CH_2OH)_2C_8H_{17})_3PMo_{12}O_{40}$ ($ILC_8$-$PMo_{12}$)* $ILC_8$-$PMo_{12}$ was synthesized in the same way as $ILC_{12}$-$PMo_{12}$ except $ILC_8$ (0.562 g) replaced $ILC_{12}$. Elemental analysis calcd. (%): C, 18.58; N, 1.69; H, 3.50. Found (%) C, 19.58; N, 1.70; H, 3.69. Yield, 0.12 g.

*Preparation of $(CH_3N(CH_2CH_2OH)_2C_4H_9)_3PMo_{12}O_{40}$ ($ILC_4$-$PMo_{12}$)* $ILC_4$-$PMo_{12}$ was synthesized in the same way as $ILC_{12}$-$PMo_{12}$ except $ILC_{12}$ was replaced by $ILC_4$ (0.461 g). Elemental analysis calcd. (%): C, 13.78; N, 1.79; H, 2.80. Found (%) C, 13.35; N, 1.76; H, 2.78. Yield, 0.11 g.

### Preparation of SWNTs-$ILC_n$ (n = 4, 8, 12)

*Preparation of SWNTs-$ILC_{12}$* Carboxylated single-walled carbon nanotubes (5 mg), $ILC_{12}$ (5 mg), dicyclohexylcarbodiimide (DCC) (10 mg) and N, N-dimethylformamide (DMF) (10 mL) are successively introduced into a 50 mL flask. The mixture was sonicated for 5 min and then intensely stirred at 50 °C for 68 h. The resulting precipitates were filtrated with a 3 μm membrane filter and washed three times with DMF, ethanol and water, respectively, then dried in air. Yield, 5.15 mg.

*Preparation of SWNTs-$ILC_8$* SWNTs-$ILC_8$ was synthesized in the same way as SWNTs-$ILC_{12}$ except $ILC_{12}$ was replaced by $ILC_8$ (0.461 g). Yield, 5.08 mg.

*Preparation of SWNTs-$ILC_4$* SWNTs-$ILC_4$ was synthesized in the same way as SWNTs-$ILC_{12}$ except $ILC_{12}$ was replaced by $ILC_4$ (0.461 g). Yield, 5.12 mg.

### Preparation of SWNTs-$ILC_n$-$PMo_{12}$ (n = 4, 8, 12)

*Preparation of SWNTs-$ILC_{12}$-$PMo_{12}$* A mixture of SWNTs-$ILC_{12}$ (5 mg) and $PMo_{12}$ (20 mg) in 20 mL of $H_2O$ was stirred for 6 h, filtered and washed with distilled water eight times. Finally, the resulting product SWNTs-$ILC_{12}$-$PMo_{12}$ was dried in air. Yield, 5.07 mg.

*Preparation of SWNTs-$ILC_8$-$PMo_{12}$* SWNTs-$ILC_8$-$PMo_{12}$ was synthesized in the same way as SWNTs-$ILC_{12}$-$PMo_{12}$ except SWNTs-$ILC_{12}$ was replaced by SWNTs-$ILC_8$ (0.461 g). Yield, 5.10 mg.

*Preparation of SWNTs-$ILC_4$-$PMo_{12}$* SWNTs-$ILC_4$-$PMo_{12}$ was synthesized in the same way as SWNTs-$ILC_{12}$-$PMo_{12}$ except SWNTs-$ILC_{12}$ was replaced by SWNTs-$ILC_4$ (0.461 g). Yield, 5.12 mg.

### Preparation of the Modified Glass Electrodes

Into a 5 mL glass vial, ethyl orthosilicate (1 mL), isopropanol (0.5 mL) and hydrochloric acid (0.1 M, 0.7 mL) were successively added, and the mixture was stirred at room temperature for 1 h, at 45 °C for 2.5 h. Adding the desired materials (1 mg) including SWNTs-$ILC_n$-$PMo_{12}$, or SWNTs-$ILC_n$, or $ILC_n$ (n = 4, 8, 12), or IL-$PMo_{12}$, or SWNTs, or $H_3PMo_{12}O_{40}$, or SWNTs/$PMo_{12}$ (mixture of SWNTs and $H_3PMo_{12}O_{40}$ in a mass ratio of 1:1) to the glass vial, sonicating for 2–3 min, and then stirring for another 0.5 h. Using a spin-coating method, a uniformly dispersed sol (10 μL) was coated on the pre-treated and activated bare glassy carbon electrode, rotated for 3 min under 600 rpm, and then naturally dried for 12 h.

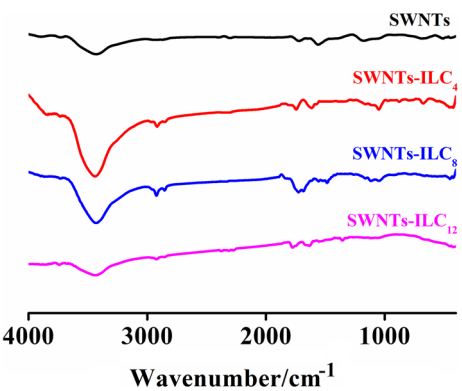


**Fig. 1** IR spectra of SWNTs-$ILC_n$ (n = 4, 8, 12)

## Results and Discussion

### FT-IR and Raman Spectra of the SWNTs-ILC$_n$ and SWNTs-ILC$_n$-PMo$_{12}$

FT-IR spectra of SWNTs, SWNTs-ILC$_4$, SWNTs-ILC$_8$ and SWNTs-ILC$_{12}$ are shown in Fig. 1, respectively. In the IR spectrum of SWNTs, the characteristic vibrational band at 1715 cm$^{-1}$ can be assigned to $\nu_{as}$ (C=O) vibration [23], and the band at 1577 cm$^{-1}$ is ascribed to the vibration of carbon skeleton of the carbon nanotubes. The IR spectra of SWNTs-ILC$_4$, SWNTs-ILC$_8$ and SWNTs-ILC$_{12}$ are similar, so the IR spectra of SWNTs-ILC$_4$ was selected as a representative to illustrate. As shown in the IR spectrum of SWNTs-ILC$_4$, the C=O stretching vibration appears at 1740 cm$^{-1}$ which is different with 1715 cm$^{-1}$ of SWNTs and the C–H stretching vibrations appear at 2973, 2919, 2844 cm$^{-1}$ which are emerging bands [24], indicating the successful formation of ester bonds between SWNTs and ILC$_4$ in the resulting SWNTs-ILC$_4$ composites. In the IR spectra of SWNTs-ILC$_n$-PMo$_{12}$ composites (n = 4, 8, 12), the bands from PMo$_{12}$ moiety cannot be well identified (Fig. 2a) due to the very low content of PMo$_{12}$ in the composites [25]. In order to confirm the presence of PMo$_{12}$ in the ternary composites, the IR spectra of IL$_n$-PMo$_{12}$ were recordered (Fig. 2b) and the main IR bands are listed in Table 1. The four characteristic IR peaks [25] of the Keggin type PMo$_{12}$ around 1064 (P–O), 960 (Mo=Ot), and 782 (Mo–Ob–Mo) and 870 cm$^{-1}$ (Mo–Oc–Mo) are clearly observed in the spectra of SWNT-IL$_n$-POM while with some red shifts for P–O and Mo=O, and blue shifts for Mo–O–Mo with respect to those of the PMo$_{12}$, respectively. The peaks around 2850 and 2920 cm$^{-1}$ are assigned to C–H vibration of the IL moieties [24]. Meantime, the elemental analysis showed that each POM bonded three IL cations, as expected. These results unequivocally suggest POM and IL are integrated, also indirectly prove that POM are integrated with SWNT-ILC$_n$ by favorable cation–anion interactions.

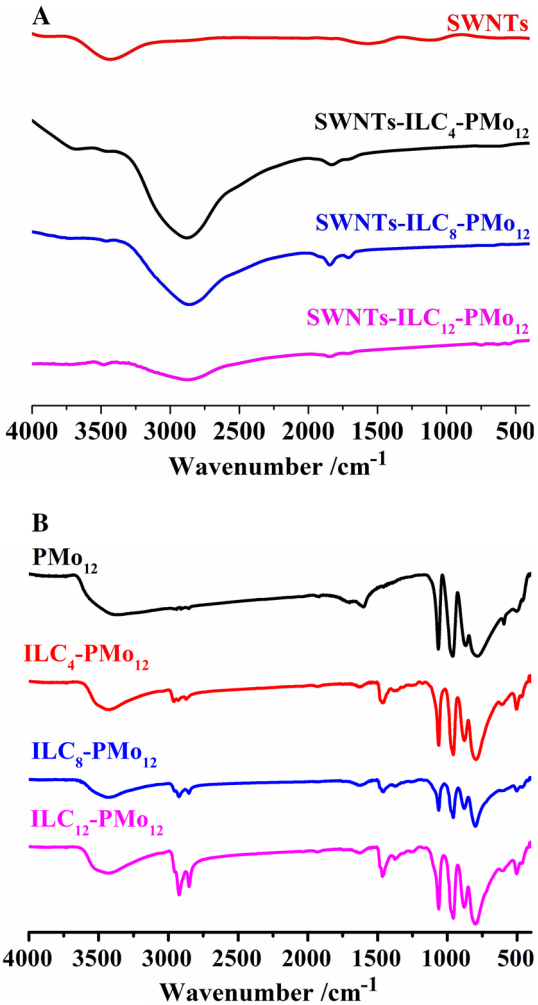


**Fig. 2** IR spectra of SWNTs-ILC$_n$-PMo$_{12}$ composites (**a**) and ILC$_n$-PMo$_{12}$ composites (**b**) (n = 4, 8, 12)

**Table 1** Main IR peaks (unit: cm$^{-1}$) and their assignments of the samples PMo$_{12}$, ILC$_{12}$-PMo$_{12}$, ILC$_8$-PMo$_{12}$ and ILC$_4$-PMo$_{12}$

| PMo$_{12}$ | ILC$_{12}$-PMo$_{12}$ | ILC$_8$-PMo$_{12}$ | ILC$_4$-PMo$_{12}$ | Assignment |
|---|---|---|---|---|
| 3402 | 3439 | 3424 | 3424 | O–H |
| | 2923, 2851 | 2924, 2853 | 2929, 2871 | C–H |
| 1700, 1601 | | | | O–H |
| | 1466 | 1466 | 1466 | C–H |
| 1064 | 1061 | 1062 | 1062 | P–O |
| 961 | 957 | 956 | 958 | M=O |
| 869 | 878 | 878 | 877 | Mo–O$_c$–Mo |
| 782 | 797 | 798 | 795 | Mo–O$_b$–Mo |

As shown in Fig. 3 and Table S1, the characteristic G band (1581 cm$^{-1}$) and radial breathing mode (RBM, 100–400 cm$^{-1}$) of the SWNTs were observed [19] in the Raman spectra of SWNTs, SWNTs-ILC$_{12}$, SWNTs-ILC$_8$, SWNTs-ILC$_4$, SWNTs-ILC$_{12}$-PMo$_{12}$, SWNTs-ILC$_8$-PMo$_{12}$ and SWNTs-ILC$_4$-PMo$_{12}$, which indicated that the original properties of the SWNT were preserved in the final composites.

### Electrochemical Impedance of Glass Carbon Electrode Modified by SWNTs-ILC$_n$-PMo$_{12}$

As we know, electrochemical impedance spectroscopy (EIS) is a powerful tool for studying the interface properties of surface-modified electrodes [26]. The electron-transfer resistance ($R_{CT}$) at the electrode surface is an

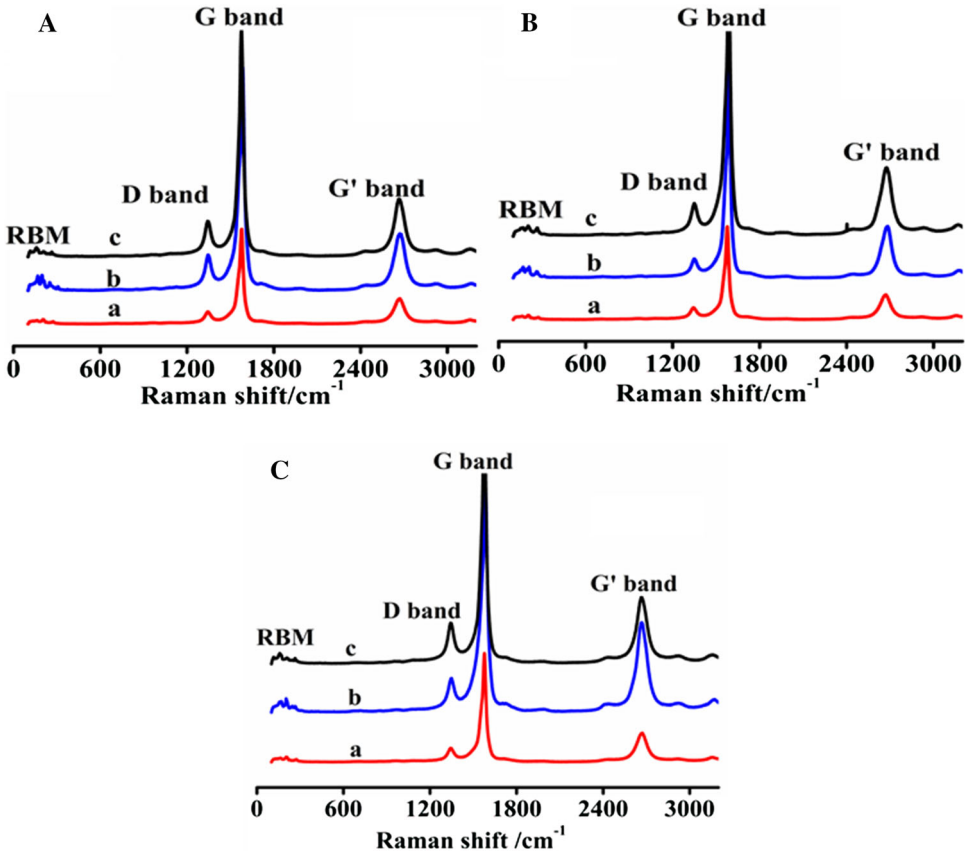


**Fig. 3** Raman spectra of SWNTs (a), SWNTs-$ILC_{12}$ (b), and SWNTs-$ILC_{12}$-$PMo_{12}$ (c) (**A**); SWNTs (a), SWNTs-$ILC_8$ (b), and SWNTs-$ILC_8$-$PMo_{12}$ (c) (**B**); and SWNTs (a), SWNTs-$ILC_4$ (b), and SWNTs-$ILC_4$-$PMo_{12}$ (c) (**C**)

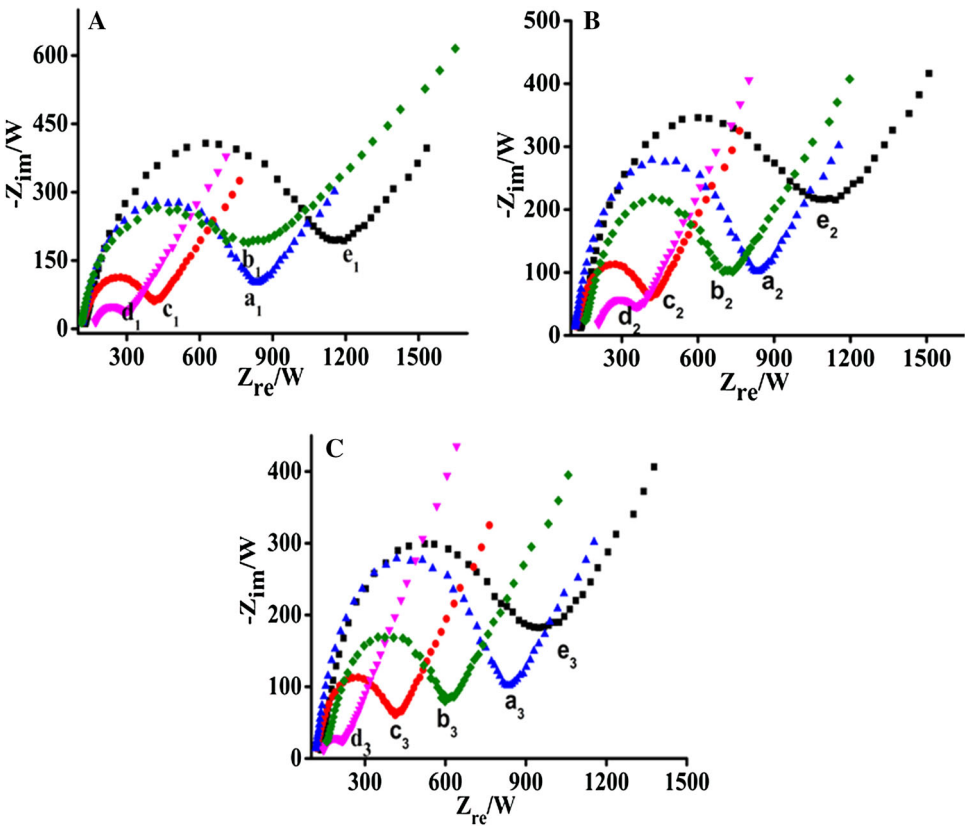


**Fig. 4** Nyquist plots of EIS for ($a_1$) bare GCE, ($b_1$) GCE/$ILC_{12}$, ($c_1$) GCE/SWNTs, ($d_1$) GCE/SWNTs-$ILC_{12}$, ($e_1$) GCE/SWNTs-$ILC_{12}$-$PMo_{12}$ (**A**); ($a_2$) bare GCE, ($b_2$) GCE/$ILC_8$, ($c_2$) GCE/SWNTs, ($d_2$) GCE/SWNTs-$ILC_8$, ($e_2$) GCE/SWNTs-$ILC_8$-$PMo_{12}$ (**B**); and ($a_3$) bare GCE, ($b_3$) GCE/$ILC_4$, ($c_3$) GCE/SWNTs, ($d_3$) GCE/SWNTs-$ILC_4$, ($e_3$) GCE/SWNTs-$ILC_4$-$PMo_{12}$ (**C**) in a solution of 5 mM $K_3Fe(CN)_6$ and 0.1 M KCl

important parameter, which can imply charge transfer rate in the material. Figure 4 showed the Nyquist plots of the impedance spectroscopy of glassy carbon electrode modified by various materials in a solution of 5 mM $K_3Fe(CN)_6$ and 0.1 M KCl. As shown in Fig. 4 and the data listed in Table S2, the impedance changes have the same pattern after the three $ILC_n$ (n = 12, 8, 4) combined with SWNTs and $PMo_{12}$. For example, the Nyquist diameter of the GCE/SWNTs ($R_{CT} \approx 246.2\ \Omega$) and GCE/$ILC_{12}$ (587.0 Ω) are all smaller than that of the GCE ($R_{CT} \approx 615.5\ \Omega$), indicating that the glassy carbon electrode modified by SWNTs or $ILC_{12}$ forms a better electron conduction pathway. Impressively, the Nyquist diameter of the GCE/SWNTs-$ILC_{12}$ ($R_{CT} \approx 125.2\ \Omega$) is smaller than GCE/SWNTs ($R_{CT} \approx 246.2\ \Omega$) and GCE/$ILC_{12}$ (587.0 Ω). The result showed that the SWNTs-IL composite film allowed greater permeation for the redox probe of $Fe(CN)_6^{3-}/^{4-}$ than the SWNTs film or $ILC_{12}$ film [26]. This was due to the synergistic effects of excellent ionic conductivity of $ILC_{12}$ [27], great electrical conductivity and large surface area of SWNTs [28], which greatly enhanced the electron transport performance of the electrode surface. SWNTs-$ILC_{12}$-$PMo_{12}$ ($R_{CT} \approx 852.5\ \Omega$) in comparison with GCE/$PMo_{12}$ ($R_{CT} \approx 6607.0\ \Omega$) showed lower interfacial resistance, this not only indicated the successful formation of the SWNTs-IL-$PMo_{12}$ composite but also demonstrated that the multifunctional composite was successfully modified onto the glassy carbon electrode. Meanwhile, the impedance in descending order of SWNTs-$ILC_{12}$-$PMo_{12}$ > SWNTs-$ILC_8$-$PMo_{12}$ > SWNTs-$ILC_4$-$PMo_{12}$, indicated that the length of alkyl chain of $ILC_n$ in the SWNTs-$ILC_n$-$PMo_{12}$ (n = 4, 8, 12) could affect the kinetic parameters and the electrode in these ordered membranes, which is similar to the findings of Miller [29] and Finklea [30] et al.

## Cyclic Voltammetry Behaviour of the Electrode Modified by SWNTs-$ILC_n$-$PMo_{12}$

Figure 5A presents the cyclic voltammograms of GCE/SWNTs-$ILC_{12}$-$PMo_{12}$, GCE/SWNTs/$PMo_{12}$, GCE/$ILC_{12}$-$PMo_{12}$ and GCE/SWNTs-$ILC_{12}$. GCE/SWNTs-$ILC_{12}$ has no redox peaks in the potential range of+ 0.6 to − 0.1 V, while GCE/SWNTs-$ILC_{12}$-$PMo_{12}$, GCE/SWNTs/$PMo_{12}$ and GCE/$ILC_{12}$-$PMo_{12}$ have three pairs of oxidation and reduction of $PMo_{12}$ through two-, four- and six-electron processes, respectively [20, 31, 32]. As shown in Fig. 5b, c, it has similar situation with $ILC_8$ and $ILC_4$ as compared with that of $ILC_{12}$. The formal potentials (E = 1/2 (Epa + Epc), the mean value of the anodic and cathodic peak potentials, peak separations ($E_p = E_{pa} - E_{pc}$) of GCE/SWNTs-$ILC_n$-$PMo_{12}$ (n = 4, 8, 12), GCE/SWNTs/$PMo_{12}$ and $ILC_n$-$PMo_{12}$ (n = 4, 8, 12) for the recorded CVs are summarized in Table S3. From the table we can see peak potential has a tendency to move in the positive direction, but the impact on the peak potential difference is not significant. Taking the third redox peak as a representative, the peak separation (Ep) at GCE/SWNTs-$ILC_{12}$-$PMo_{12}$ (0.014 V) is smaller than GCE/SWNTs/$PMo_{12}$ (0.019 V) and GCE/$ILC_{12}$-$PMo_{12}$ (0.018 V), which indicated that the ionic conductivity of the $ILC_n$ (n = 4, 8, 12) and the excellent electronic conductivity of the SWNTs played an important role in the electron transfer on the surface of the electrode, thus made the electron-transfer on the electrode surface faster [26, 27], which is in accordance with the results from impedance experiments. At the same time, it can be noticed that the peak currents of GCE/SWNTs-$ILC_{12}$-$PMo_{12}$, GCE/SWNTs/$PMo_{12}$ and GCE/$ILC_{12}$-$PMo_{12}$ were slightly different due to the different content of phosphomolybdic acid.

Figure 6 shows the cyclic voltammograms at different scan rates for SWNTs-$ILC_{12}$-$PMo_{12}$, SWNTs-$ILC_8$-$PMo_{12}$ and SWNTs-$ILC_4$-$PMo_{12}$ modified glassy carbon electrodes, respectively. The results implied that all the peak potentials and the peak separations of the modified electrodes do not change with the scan rate between − 0.15 and 0.6 V. The reduction peak current and the oxidation peak current increased linearly at scan rates of 0.01 to 1 V $s^{-1}$, indicating that the rate of electrode reactions is controlled by the electrochemical steps on the surface [20].

## 3.4 pH-Dependent Electrochemical Behaviour of the GCE/SWNTs-$ILC_n$-$PMo_{12}$ (n = 4, 8, 12)

In general, the reduction of POMs is accompanied by protonation, therefore, the electrochemical behaviour of POMs relies on the pH of the solution to a large extent. In order to study the protonation process of POMs with the introduction of SWNTs-IL, the CV curve of GCE/SWNTs-$ILC_{12}$-$PMo_{12}$, GCE/SWNTs-$ILC_8$-$PMo_{12}$ and GCE/SWNTs-$ILC_4$-$PMo_{12}$ at different pHs have been done. From Fig. 7, we can see that along with increasing PH, the three redox potentials all gradually shifted to the negative potential direction, a result similar with reported in literature [20]. The reduction of $PMo_{12}$ occurs when the protons in solution migrate to the electroactive material on the modified electrode [31]. Along with increasing pH, the $H^+$ concentration decreased, then the redox current decreased, and the more negative reduction potentials can be elucidated by the Nernst equation [33].

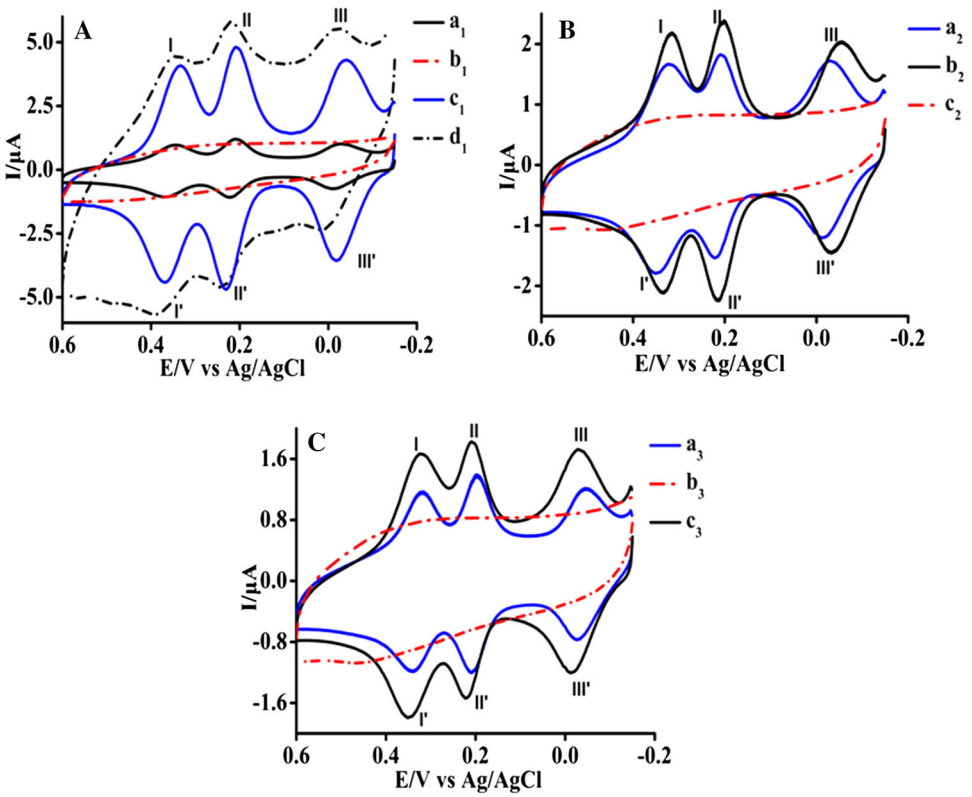


**Fig. 5** Cyclic voltammograms for ($a_1$) GCE/SWNTs-$ILC_{12}$-$PMo_{12}$, ($b_1$) GCE/SWNTs-$ILC_{12}$, ($c_1$) GCE/$ILC_{12}$-$PMo_{12}$ and ($d_1$) GCE/SWNTs/$PMo_{12}$ (**A**); ($a_2$) GCE/SWNTs-$ILC_8$-$PMo_{12}$, ($b_2$) GCE/SWNTs-$ILC_8$, ($c_3$) GCE/$ILC_8$-$PMo_{12}$ (**B**); and ($a_3$) GCE/SWNTs-$ILC_4$-$PMo_{12}$, ($b_3$) GCE/SWNTs-$ILC_4$, ($c_3$) GCE/$ILC_4$-$PMo_{12}$ in 0.5 M $H_2SO_4$ solution at a scan rate of 100 mV $s^{-1}$

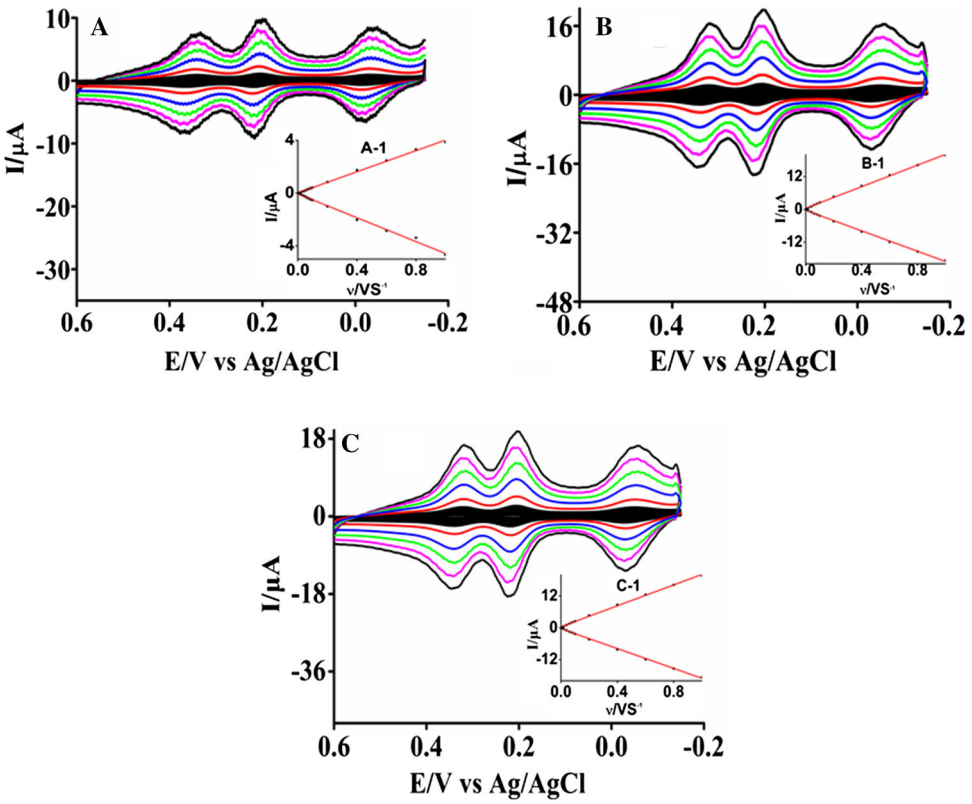


**Fig. 6** Cyclic voltammograms of SWNTs-$ILC_{12}$-$PMo_{12}$ (**A**, A-1), SWNTs-$ILC_8$-$PMo_{12}$ (**B**, B-1), and SWNTs-$ILC_4$-$PMo_{12}$ (**C**, C-1) in 0.5 M $H_2SO_4$ at scan rates of 10–1000 mV $s^{-1}$ from inner to outer and the dependence of peak currents (III) on scan rates

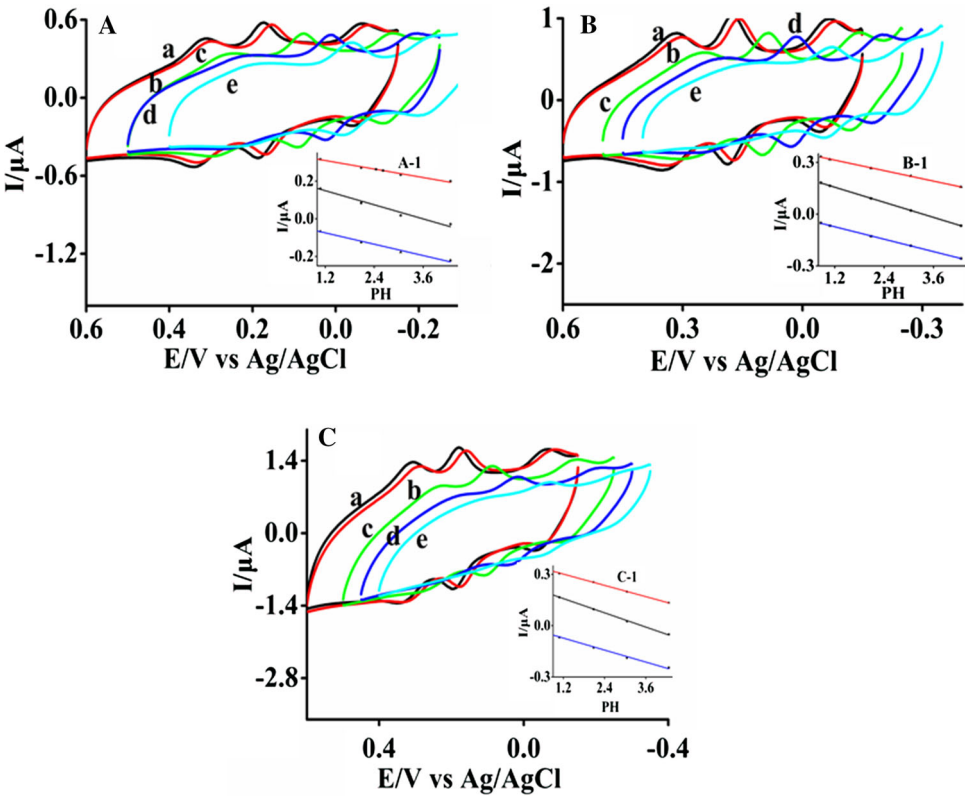


**Fig. 7** Cyclic voltammograms of a SWNTs-ILC$_{12}$-PMo$_{12}$ (**A**), SWNTs-ILC$_8$-PMo$_{12}$ (**B**), SWNTs-ILC$_4$-PMo$_{12}$ (**C**) at different pHs (from a to e: 0.86, 1.08, 2.08, 3.05 and 4.27; a: black, b: red, c: green, d: blue, e: cyan) and at a scan rate of 50 mV s$^{-1}$. The insets (A-1 in (**A**); B-1 in (**B**) and C-1 in (**C**)) show variation of potentials as a function of pH for three redox pairs I–Í (red line), II–IÍ (black line) and III–IIÍ (blue line) (Color figure online)

The electrochemical reaction of PMo$_{12}$-doped electrode can be shown as follows:

$$PMo_{12}O_{40}^{3-} + 2e^- + 2H^+ = H_2Mo_{10}^{VI}PMo_2^{V}O_{40}^{3-}$$
$$H_2Mo_{10}^{VI}PMo_2^{V}O_{40}^{3-} + 2e^- + 2H^+ = H_4Mo_8^{VI}PMo_4^{V}O_{40}^{3-}$$
$$H_4Mo_8^{V}IPMo_4^{V}O_{40}^{3-} + 2e^- + 2H^+ = H_6Mo_6^{VI}PMo_6^{V}O_{40}^{3-}$$

## Electrode Stability and Storage Stability

Long term stability is one of the most important properties of sensors, biosensors and bioreactors [26]. The stability of the modified electrode which stayed at room temperature in the air was determined by comparing the changes in voltammetric peak currents before and after 100 cycles scanning in $H_2SO_4$ (0.5 M) solution at 50 V s$^{-1}$. Figure S1 shows the reduction peak currents (II-II') of the CV curve of SWNTs-ILC$_{12}$-PMo$_{12}$ modified electrode which is stable at the 1st and 100th cycles, and the current was reduced by 9.4% after 100 cycles. One week later, it was reduced by 12.4% after 100 cycles, indicating the electrode shows better stability in the electrolyte solution. This can be attributed to SWNTs, ionic liquids and polyoxometalates are chemically bonded together successfully, which avoid leakage of POM into solution. When we replaced ILC$_{12}$ by ILC$_8$ and ILC$_4$, the current decreased as 8.2% and 7.5% after 100 cycles, respectively, which also has better stability.

## Catalytic Reduction of $IO_3^-$, $BrO_3^-$ and $NO_2^-$

Iodate, bromate and nitrite exist in many environments and are closely related to daily life and health of human beings, therefore catalytic reduction and detection is important in both theoretical and practical point of view [34–36]. The catalytic reduction of $IO_3^-$, $BrO_3^-$ and $NO_2^-$ by the modified glass carbon electrode can be seen clearly in Fig. 8, Fig. S2 and Fig. S3, respectively. Compared with the CV curve without $IO_3^-$, $BrO_3^-$ and $NO_2^-$, the reduction peak currents of the second and third pairs markedly increased by the addition of them, while the corresponding oxidation peak currents decreased comparably. Also note that there was less variation in the current of the first pair of redox peaks, irrespective of the addition of anions. This indicated that the second and third pair of redox peaks of SWNTs-ILC$_{12}$-PMo$_{12}$, SWNTs-ILC$_8$-PMo$_{12}$ and SWNTs-ILC$_4$-PMo$_{12}$ modified glassy carbon electrodes have good electrocatalysis effect.

The $IO_3^-$, $BrO_3^-$ and $NO_2^-$ are reduced by the four-electron- and six-electron-reduced PMo$_{12}$ species, respectively. The electrocatalytic behaviour above are tentatively explained by the following mechanism [37–39]:

$$3H_4Mo_8^{VI}PMo_4^{V}O_{40}^{3-} + IO_3^- \rightarrow 3H_2Mo_{10}^{VI}PMo_2^{V}O_{40}^{3-} + 3H_2O + I^-$$
$$3H_6Mo_6^{VI}PMo_6^{V}O_{40}^{3-} + 2IO_3^- \rightarrow 3H_2Mo_{10}^{VI}PMo_2^{V}O_{40}^{3-} + 6H_2O + 2I^-$$
$$3H_4Mo_8^{VI}PMo_4^{V}O_{40}^{3-} + BrO_3^- \rightarrow 3H_2Mo_{10}^{VI}PMo_2^{V}O_{40}^{3-} + 3H_2O + Br^-$$
$$3H_6Mo_6^{VI}PMo_6^{V}O_{40}^{3-} + BrO^{3-} \rightarrow 3H_4Mo_8^{VI}PMo_4^{V}O_{40}^{3-} + 3H_2O + Br^-$$
$$H_4Mo_8^{VI}PMo_4^{V}O_{40}^{3-} + NO_2^- \rightarrow H_2Mo_{10}^{VI}PMo_2^{V}O_{40}^{3-} + H_2O + N^- \text{ containing products}$$
$$H_6Mo_6^{VI}PMo_6^{V}O_{40}^{3-} + NO_2^- \rightarrow H_2Mo_{10}^{VI}PMo_2^{V}O_{40}^{3-} + H_2O + N^- \text{ containing products.}$$

The current of second reduction peak changed linearly with the concentration of $IO_3^-$ in the range of 48–167 μM, the linear equations are: $y = 0.273 + 2.933x$ (II, Linear correlation coefficient, $r^2 = 0.997$) for SWNTs-ILC$_{12}$-PMo$_{12}$, $y = 0.253 + 6.356x$ (II, $r^2 = 0.995$) for SWNTs-ILC$_8$-PMo$_{12}$, $y = 0.147 + 15.431x$ (II, $r^2 = 0.997$) for SWNTs-ILC$_4$-PMo$_{12}$, respectively. In the concentration range of $BrO_3^-$ between 4.76 and 20.00 mM, the second reduction peak catalytic current varied linearly with $BrO_3^-$ concentration, the linear equations are: $y = 0.302 + 0.020x$ (II, $r^2 = 0.997$) for SWNTs-ILC$_{12}$-PMo$_{12}$, $y = 0.276 + 0.055x$ (II, $r^2 = 0.995$) for SWNTs-ILC$_8$-PMo$_{12}$, $y = 0.455 + 0.124x$ (II, $r^2 = 0.995$) for SWNTs-ILC$_4$-PMo$_{12}$, respectively. For $NO_2^-$ of the concentration between 0.407 and 2.000 mM, the catalytic current also changes linearly with concentration of $NO_2^-$, the linear equations are $y = 0.298 + 0.09x$ (II, $r^2 = 0.987$) for SWNTs-ILC$_{12}$-PMo$_{12}$, $y = 0.289 + 0.149x$ (II, $r^2 = 0.979$) for SWNTs-ILC$_8$-PMo$_{12}$, $y = 0.329 + 0.236x$ (II, $r^2 = 0.984$) for

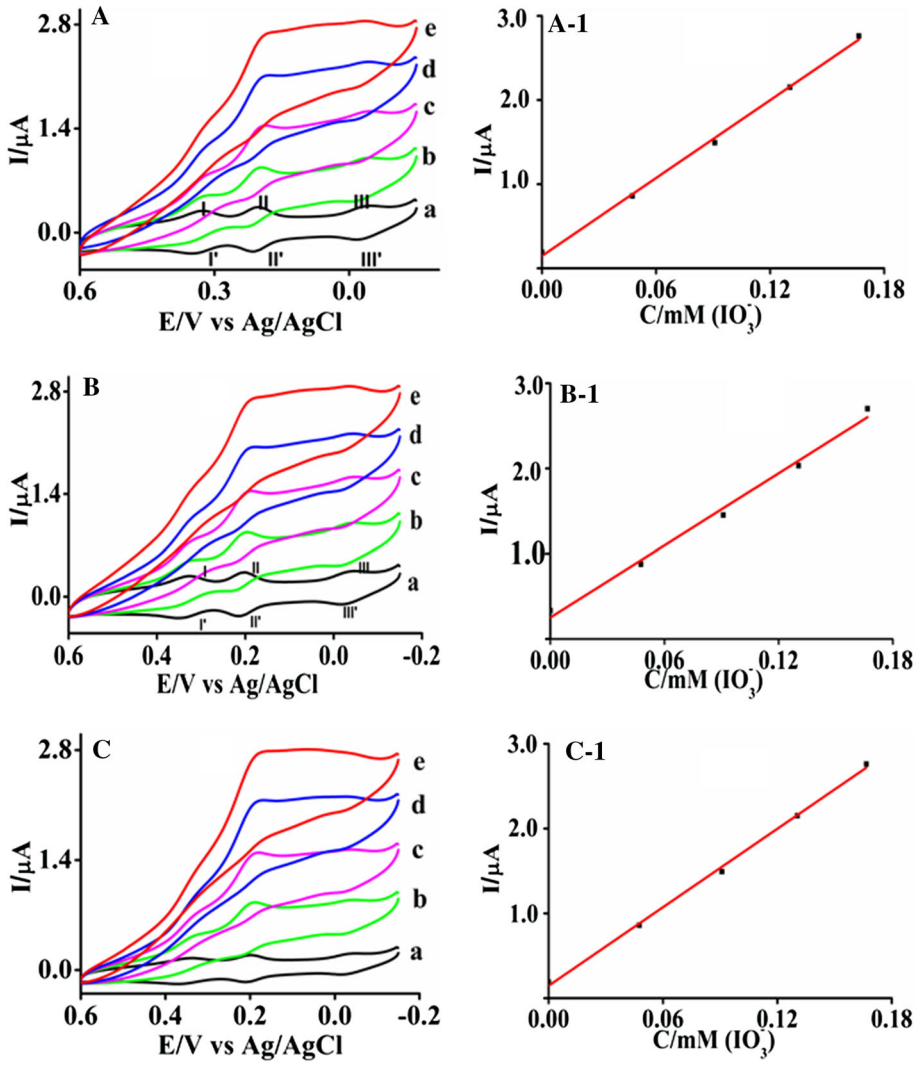


**Fig. 8** Cyclic voltammograms of the SWNTs-ILC$_{12}$-PMo$_{12}$ (**A**, A-1), SWNTs-ILC$_8$-PMo$_{12}$ (**B**, B-1), SWNTs-ILC$_4$-PMo$_{12}$ (**C**, C-1) in 0.5 M $H_2SO_4$ containing 0, 0.048, 0.091, 0.130, 0.167 mM $NaIO_3$. Scan rate 10 mV $s^{-1}$. Diagram showing variation of the reduction peak (II) current versus concentration change of $NaIO_3$ (A-1, B-1, C-1)

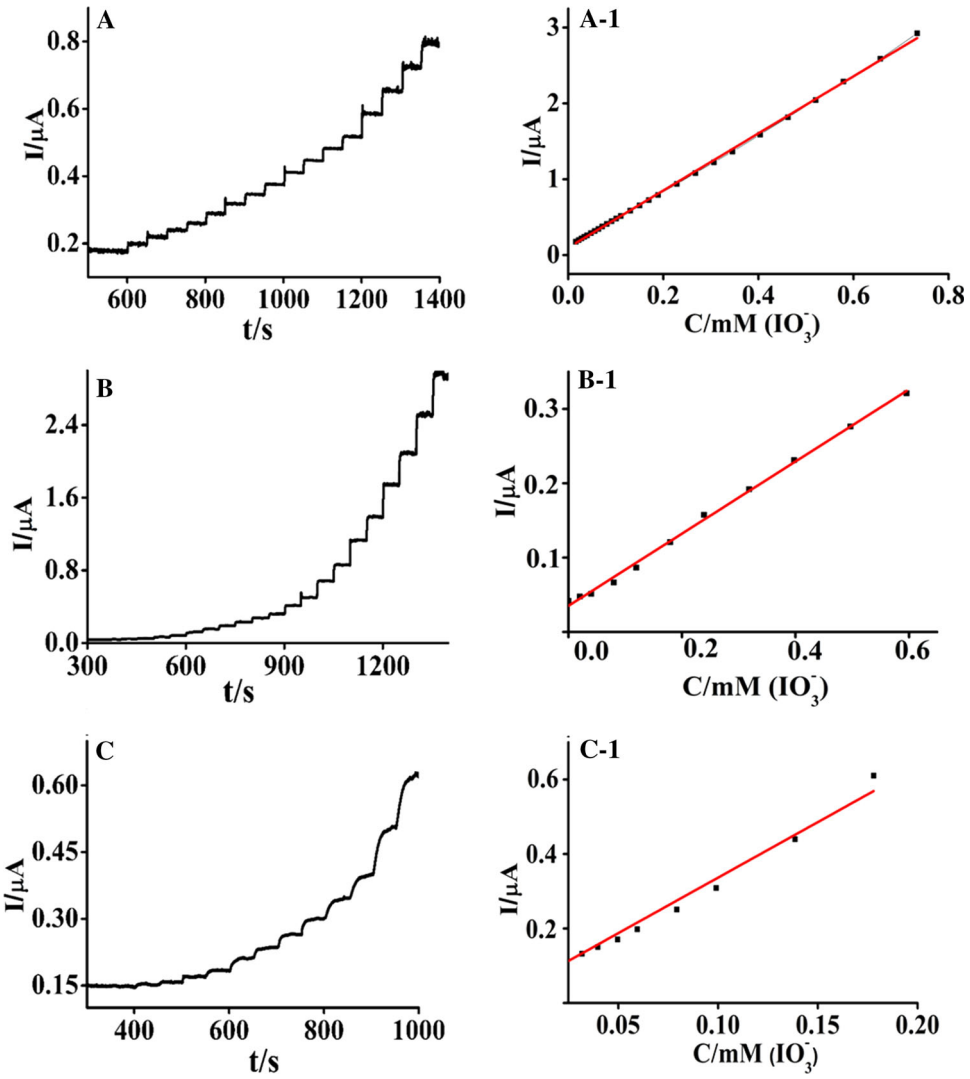


**Fig. 9** Amperometric response of the SWNTs-ILC$_{12}$-PMo$_{12}$ (A, A-1), SWNTs-ILC$_8$-PMo$_{12}$ (B, B-1), SWNTs-ILC$_4$-PMo$_{12}$ (C, C-1) and the calibration curve for steady-state current versus sodium iodate concentration, respectively. Condition: successive addition four times of sodium iodate solution ($4 \times 10^{-3}$, $6 \times 10^{-3}$, $8 \times 10^{-3}$, $1 \times 10^{-2}$, $2 \times 10^{-2}$, $4 \times 10^{-2}$, $6 \times 10^{-2}$, $8 \times 10^{-2}$, $1 \times 10^{-1}$ mol L$^{-1}$) to 20 mL 0.5 M $H_2SO_4$ (20 μL each time, interval: 50 s)

SWNTs-ILC$_4$-PMo$_{12}$, respectively. It is clear that that when n (the length of alkyl carbon chain) of the ionic liquid decreased, the slope of the linear equation became large, i.e., the sensitivity of the catalytic current gradually increased.

## The Detection of Iodate, Bromate and Nitrite

Electrochemical sensors have the advantages of high sensitivity, rapid detection, simple instruments and easy portability as compared with the other techniques [40]. Considering the above electrocatalytic reduction performance of the GCE/SWNTs-ILC$_n$-PMo$_{12}$ on iodate, bromate and nitrite, the possibility as amperometric sensors is investigated in order to measure the contents of iodide, bromate and nitrite by chronoamperometry.

Figure 9 shows the curves of current versus time and steady-state peak current versus $IO_3^-$ concentration by chronoamperometry for three different modified electrodes. From the data listed in Table S4, it is known that the linear range (LDR) of $NaIO_3$ detection by GCE/SWNTs-ILC$_n$-PMo$_{12}$ are 0.004–0.73 mM (n = 12), 0.008–0.59 mM(n = 8) and 0.008–0.19 mM (n = 4) with response time 2.5 s, 2.8 s and 2.9 s, and detection limit 0.9 μM, respectively. Compared with the others reported in literatures (Table S4), it can be concluded that GCE/SWNTs-ILC$_n$-PMo$_{12}$, especially in the case of n = 12, has a fast response, a wide linear range, and a low detection limit. The main reason must be due to the high specific surface area and strong conductivity of SWNTs, as well as the synergistic interaction with ionic liquids, resulting in high conductivity and high electrocatalytic activity of the composites [33]. This showed that the addition of carbon nanotubes and ionic liquids enhanced the detection performance of phosphomolybdic acid. Notably, the ion interference test performed on this modified electrode showed that $Ba^{2+}$ and $Mg^{2+}$ ($C(M^{2+})/C(IO_3^-) > 200$) and $Na^+$, $Cl^-$ ($C(NaCl)/C(IO_3^-) > 2000$), did not interfere with the test of $IO_3^-$. Fig. S4 and data listed in Table S5 showed that the linear

range (LDR) of $NaBrO_3$ detection by GCE/SWNTs-$ILC_n$-$PMo_{12}$ (n = 12, 8 and 4) were: 0.2–3.84 mM, 0.2–2.64 mM, 0.2–1.71 mM; Response time: 3.6 s, 4.0 s, 4.2 s; Sensitivity: 0.023 μA $Mm^{-1}$, 0.045 μA $Mm^{-1}$, 0.104 μA $Mm^{-1}$, respectively, for n = 12, 8, and 4. From Fig. S5 and data listed in Table S6, it is known that the linear range (LDR) of $NaNO_2$ detection were: 0.02–4.33 mM, 0.02–1.58 mM, 0.02–0.99 mM; Response time: 5.8 s, 6.1 s, 6.5 s; Sensitivity: 0.19 μA $Mm^{-1}$, 0.29 μA $Mm^{-1}$, 0.43 μA $Mm^{-1}$, respectively, for n = 12, 8, and 4. Based on the above results, it can be concluded that GCE/SWNTs-$ILC_{12}$-$PMo_{12}$ has a fast response, a wide linear range, and a low detection limit as compared with the other two. With the increase of n (the length of alkyl carbon chain) on the liquid $ILC_n$, it leads to an increasingly linear detection range for $NaIO_3$, $NaBrO_3$ and $NaNO_2$, which is due to that the length of carbon chain influences the kinetic parameters of the electrode surface reaction, and the long-chain film has good ordered arrangement [41]. However, with the increase of the alkyl carbon chain length—n on the ionic liquid, its sensitivity to $NaIO_3$ gradually decreases, mainly due to the resistance increases with the increase of the carbon chain length (see Table S2) that causes the detection of current to become low.

## Conclusions

In this work three new ternary composites were obtained by functionally modifying the anionic and cationic moieties of ethanolamine ionic liquids with phosphomolybdic acid and carboxylated single-walled carbon nanotubes, and then the glassy carbon electrode was modified with the composites by spin-coated method. It is revealed that the electronic conductivity of SWNTs moiety and ionic conductivity of ILs moiety played key roles on the electrocatalysis performance of composites, and the length of alkyl carbon chain of ILs also had a notable effect. While all the ternary composites modified electrodes showed remarkable catalytic activity towards the reduction/detection of iodate, bromate and nitrite, the SWNTs-$IL_{12}$-$PMo_{12}$ modified electrode showed a little bit better stability and electro-catalytic activity and sensor performance (low detection limit, short response time and wide linear range) toward iodate, borate and nitrite than the other two composites probably due to that the long-chain film had better ordered arrangement. We believe that through the double modification of ionic liquids with cations and cations, various new multifunctional materials can be designed and synthesized, which are expected to be applied in many fields.

**Acknowledgements** The financial support of the Natural Science Foundation of China is greatly acknowledged. Prof. Xue Duan, Beijing University of Chemical Technology, is greatly acknowledged for his kind support.

## References

1. M. Galiński, A. Lewandowski, and I. Stępniak (2006). *Electrochim. Acta* **51**, 5567.
2. R. D. Rogers and K. R. Seddon (2003). *Science* **302**, 792.
3. A. P. Abbott, G. Capper, D. L. Davies, H. L. Munro, R. K. Rasheed, and V. Tambyrajah (2001). *Chem. Commun.* **19**, 2010.
4. P. Wasserscheid and W. Keim (2000). *Angew. Chem. Int. Ed.* **39**, 3772.
5. S. V. Dzyuba and R. A. Bartsch (2001). *Chem. Commun.* **16**, 1466.
6. T. Hirashige, R. Hagiwara, and Y. Ito (2000). *J. Fluorine Chem.* **106**, 205.
7. J. C. Xiao and J. N. M. Shreeve (2005). *J. Org. Chem.* **70**, 3072.
8. X. H. Li, D. B. Zhao, Z. F. Fei, and L. F. Wang (2006). *Sci. China Ser. B Chem.* **36**, 181.
9. A. Dolbecq, E. Dumas, C. R. Mayer, and P. Mialane (2010). *Chem. Rev.* **110**, 6009.
10. Y. H. Sun, L. I. Xiao-Ping, Z. M. Mei, Y. Zhu, and L. Niu (2011). *Chem. Res. Chin. Univ.* **27**, 6.
11. Y. W. Li, Y. G. Li, Y. H. Wang, X. J. Feng, Y. Lu, and E. B. Wang (2009). *Inorg. Chem.* **48**, 6452.
12. G. Hou, L. Bi, B. Li, and L. Wu (2010). *Inorg. Chem.* **49**, 6474.
13. R. Thangamuthu, Y. C. Pan, and S. M. Chen (2010). *Electroanalysis.* **22**, 1812.
14. J. D. Kim, S. Hayashi, T. Mori, and I. Honma (2007). *Electrochim. Acta* **53**, 963.
15. X. Wu, W. Wu, Q. Wu, and W. Yan (2017). *Langmuir.* **33**, 4242.
16. L. Hu, D. S. Hecht, and G. Grüner (2010). *Chem. Rev.* **110**, 5790.
17. A. Sun, J. Zheng, and Q. Sheng (2012). *Electrochim. Acta* **65**, 64.
18. Y. Li, X. Liu, X. Liu, N. Mai, Y. Li, W. Wei, and Q. Cai (2011). *B Biointerfaces* **88**, 402.
19. Y. Zhang, Y. Shen, J. Yuan, D. Han, Z. Wang, Q. Zhang, and L. Niu (2006). *Angew. Chem. Int. Ed.* **45**, 5867.
20. B. Haghighi, H. Hamidi, and L. Gorton (2010). *Electrochim. Acta* **55**, 4750.
21. B. K. Mishra, P. Mukherjee, S. Dash, S. Patel, and H. N. Pati (2009). *Inorg. Chem.* **39**, 2529.
22. S. Roy, A. Dasgupta, and P. K. Das (2006). *Langmuir* **22**, 4567.
23. L. Liu, Y. Qin, Z. X. Guo, and D. Zhu (2003). *Carbon* **41**, 331.
24. E. Rogelhernández, G. Alonsonuñez, J. P. Camarena, H. Espinozagómez, G. Aguirre, F. Paraguaydelgado, and R. Somanathan (2011). *J. Mex. Chem. Soc.* **55**, 7.
25. R. Claude, F. Michel, F. Raymonde, and T. Rene (1983). *Inorg. Chem.* **22**, 207.
26. W. Guo, L. Xu, F. Li, B. Xu, Y. Yang, S. Liu, and Z. Sun (2010). *Electrochim. Acta* **55**, 1523.
27. S. D. L. Cruz, M. D. Green, Y. Ye, Y. A. Elabd, T. E. Long, and K. I. Winey (2012). *J. Polym. Sci. Part A: Polym. Chem.* **50**, 338.
28. Z. Xu, N. Gao, and S. Dong (2006). *Talanta* **68**, 753.
29. J. Cheng, G. Sàghiszabó, J. A. T. And, and C. J. Miller (1996). *J. Am. Chem. Soc.* **118**, 680.
30. H. O. Finklea and D. D. Hanshew (1992). *J. Am. Chem. Soc.* **114**, 3173.
31. P. Wang, X. Wang, and G. Zhu (2000). *Electroanalysis* **12**, 1493.
32. Z. Li, J. Chen, D. Pan, W. Tao, L. Nie, and S. Yao (2006). *Electrochim. Acta* **51**, 4255.

33. T. Peter *Laboratory Techniques in Electroanalytical Chemistry* (Dekker, New York, 1984).
34. L. Guadagnini and D. Tonelli (2013). *Sens. Actuators B Chem.* **188**, 806.
35. A. Salimi, A. Noorbakhsh, and M. Ghadermarzi (2006). *Sens. Actuators B Chemical* **1**, 530.
36. A. Salimi, V. Alizadeh, and H. Hadadzadeh (2010). *Electroanalysis* **16**, 1984.
37. W. Song, X. Chen, Y. Jiang, Y. Liu, C. Sun, and X. Wang (1999). *Anal. Chim. Acta* **394**, 73.
38. L. Li, W. Li, C. Sun, and L. Li (2002). *Electroanalysis* **14**, 368.
39. L. D. Li, W. J. Li, and C. Q. Li (2000). *Chem. J. Chin. Univ.* **21**, 865.
40. T. Dong, F. Chen, J. Du, and C. Hu (2010). *J. Cluster Sci.* **21**, 779.
41. L. Liu, S. Y. Song, and P. Y. Zhang (2012). *Acta Phys. Chim. Sin.* **28**, 427.